ROYAL SOCIETY OF CHEMISTRY

PAPER

Check for updates

Diphenylamine substituted 5,6,12, 13-tetraazaperopyrene based polymorphic microcrystals versatile in multi-directional isotropic and anisotropic photon transport†

Di Tian,[a] Chaofei Xu,[c] Wei Yuan,[ab] Xue-Dong Wang [ID] *[c] and Yulan Chen [ID] *[ab]

Geometrically well-defined microcrystals with polymorphic tailorability are in high demand for multi-directional photon flow at the microscale. Herein, diphenylamine (DPA) substituted 5,6,12,13-tetraazaperopyrene **c-TAPP-DPA** is synthesized and explored as a versatile fluorophore to fabricate polymorphic microcrystals for photonic applications. The flexibly twisted and electron rich DPA groups are verified as a crucial structure element to tune the intermolecular interactions and packing modes of **c-TAPP-DPA**, resulting in three kinds of crystals, including microrods, and rhomboid and hexagonal microplates. These microcrystals display geometry-dependent fluorescence properties and 1D or 2D waveguide properties with low optical loss. Impressively, the micro-rhomboids show a unique 2D asymmetric waveguide character. Our work enriches the diversity of polymorphic microcrystals, and sheds more light on the structure–property relationship of organic crystals for multi-directional optical waveguide applications.

Introduction

Directional control of photonic waveguides can pave the way to the development of integrated optical circuits.[1–4] Organic micro/nano-crystals with ordered structures and excellent optical properties have become ideal candidates for optical waveguides,[2,5–9] lasers,[10–15] and light-emitting transistors.[16–19] A wealth of structures and optical properties of organic fluorophores offer broad opportunities to modulate the resultant crystal structures and functionalities.[20–23] Of particular importance is the shape and dimension controls of the crystals for confining and guiding photonic flow with low loss, which greatly rely on the molecular structures and packing modes of the fluorophores.[24–28] Notably, polymorphism with two or more crystalline phases stemming from one organic molecule can greatly enrich the types of micro/nano-crystals for excellent photonic properties; meanwhile it provides a sophisticated

platform to shed more light on the relationship between molecular stacking patterns and solid-state optical properties.[29–35]

Apart from the polymorphic control of multimodal and low loss optical waveguides, 2D crystals capable of anisotropic propagation of photons, with multiple channels showing different polarization and emission properties, are also in high demand due to their considerable potential in optical planar diodes, logic devices, *etc.*[2,36–42] Although it has been recognized that the fabrication of 2D organic crystals with anisotropic features is pertinent to the molecular-packing modes with controlled transition dipole of molecules in crystals, most reported 2D organic crystals exhibited isotropic photon propagation behaviors.[43,44] In this regard, the development of versatile photonic fluorophores with packing modes and transition dipoles suitable for polymorphic micro/nano-crystals and anisotropic 2D photon transport is of great significance, whereby fine-tuning the intermolecular interactions is crucial, yet remains challenging.

Our previous study has showed that 5,6,12,13-tetraazaperopyrene (TAPP) was a unique photonic fluorophore.[45] N-doping and *t*-Bu substitution enabled a precise control of intermolecular interactions. However, the *t*-Bu substituted TAPPs can neither fabricate polymorphic micro/nano-crystals, nor feature anisotropic 2D photon propagation. To address this limitation, appropriate substitution of the TAPP core, by introducing steric electron-donating groups, is expected to be a necessity to synergistically tune the intermolecular interactions, frontier orbital energies, and the photophysical and photonic properties of the

[a] *Department of Chemistry, Tianjin Key Laboratory of Molecular Optoelectronic Science, Tianjin University, Tianjin, 300354, P. R. China. E-mail: yulanchen@jlu.edu.cn*

[b] *State Key Laboratory of Supramolecular Structure and Materials, College of Chemistry, Jilin University Changchun, 130012, P. R. China*

[c] *Institute of Functional Nano & Soft Materials (FUNSOM), Jiangsu Key Laboratory for Carbon-Based Functional Materials & Devices, Soochow University Suzhou, 215123, P. R. China. E-mail: wangxuedong@suda.edu.cn*
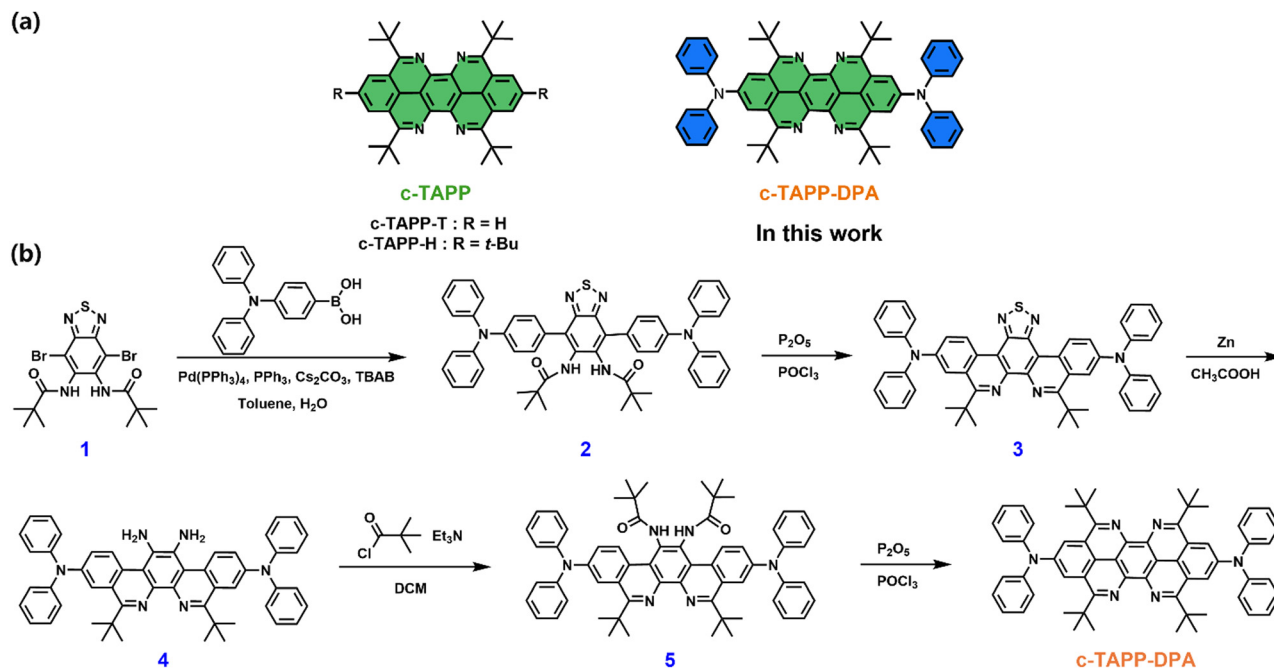
Scheme 1 (a) Chemical structures of substituted 5,6,12,13-tetraazaperopyrenes in previous work and in this work; (b) the synthesis of **c-TAPP-DPA**.

resultant fluorophores. In this contribution, we therefore synthesized a diphenylamine substituted TAPP for polymorph engineering and photonic applications (**c-TAPP-DPA**, Scheme 1a). Electronic (electron rich) and conformational (steric and twisting) effects offered by diphenylamine groups endowed **c-TAPP-DPA** with intrinsic intramolecular charge transfer (ICT) characteristic with the ability to form polymorphic micro/nano-crystals ranging from 1D microrods to 2D rhomboid and hexagonal microplates. These microcrystals exhibited different molecular packing patterns, which eventuate in their different fluorescence and optical waveguide properties. Remarkably, the rhomboid microplates displayed an anisotropic photonic behavior. This work thus enriched the structural and functional diversity of organic photonic fluorophores.

Results and discussion

The target molecule **c-TAPP-DPA** was synthesized *via* a stepwise four-fold Bischler–Napieralski cyclization as the key step

Fig. 1 (a) Normalized UV-vis absorption and FL emission spectra of **c-TAPP-DPA** in toluene (2.0×10^{-5} M). (b) Frontier molecular orbitals of **c-TAPP-DPA** calculated by density functional theory (DFT) studies.

(Scheme 1b), a similar protocol to that for **c-TAPP** preparation, except for the choice of 4-(diphenylamino)phenylboronic acid as one of the starting reagents. All intermediates and the product were characterized by mass and NMR (^{1}H and ^{13}C) spectroscopy. Good thermal stability of **c-TAPP-DPA** was confirmed by TGA measurement (Fig. S1, ESI†).

In toluene, **c-TAPP-DPA** showed well-resolved intense UV-visible absorption bands peaks at 411 ($\varepsilon = 2.3 \times 10^4$ M^{-1} cm^{-1}), 437 ($\varepsilon = 4.8 \times 10^4$ M^{-1} cm^{-1}) and 465 ($\varepsilon = 6.1 \times 10^4$ M^{-1} cm^{-1}) nm, respectively, that can typically be seen for the π–π* transition in the peropyrene scaffold (Fig. 1a). Compared to **c-TAPP**, an additional absorption band at *ca.* 520 nm was observed, assignable to weak ICT transition in **c-TAPP-DPA** from the electron-donating DPA moieties to the TAPP core. The toluene solution of **c-TAPP-DPA** emitted yellow FL with a maximum at 534 nm and an absolute quantum yield of 42% (Table S1, ESI†). Both the characteristic absorption and FL peaks were bathochromically shifted by about 9 nm and 37 nm, respectively, with respect to the *t*-Bu substituted **c-TAPP**, which can be attributed to the conjugation between the TAPP core and the two electron-rich substituents. Besides, the solvatochromic effect was verified, in particular, for that in excited state. That was, for the ICT absorption band, and more remarkably for the FL bands, they were red-shifted with solvent polarity increasing, corresponding to classic ICT characteristics. (Fig. S2, ESI†)

Fig. 1b was the calculated frontier orbitals of **c-TAPP-DPA** based on DFT modelling. The results supported the interpretation that **c-TAPP-DPA** was an intramolecular donor–acceptor molecule: the HOMO was localized mainly on the peripheral DPA substituents, whereas a more significantly uneven distribution was found for the LUMO that was typically localized at the peropyrene core. The observed charge-transfer band (*vide supra*)
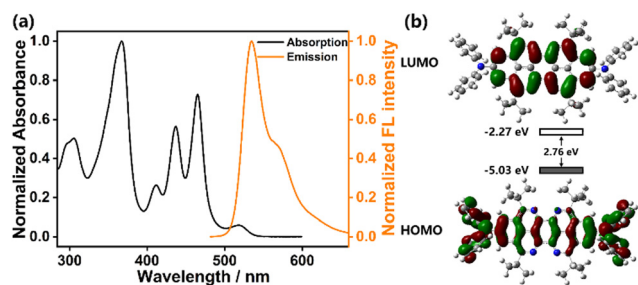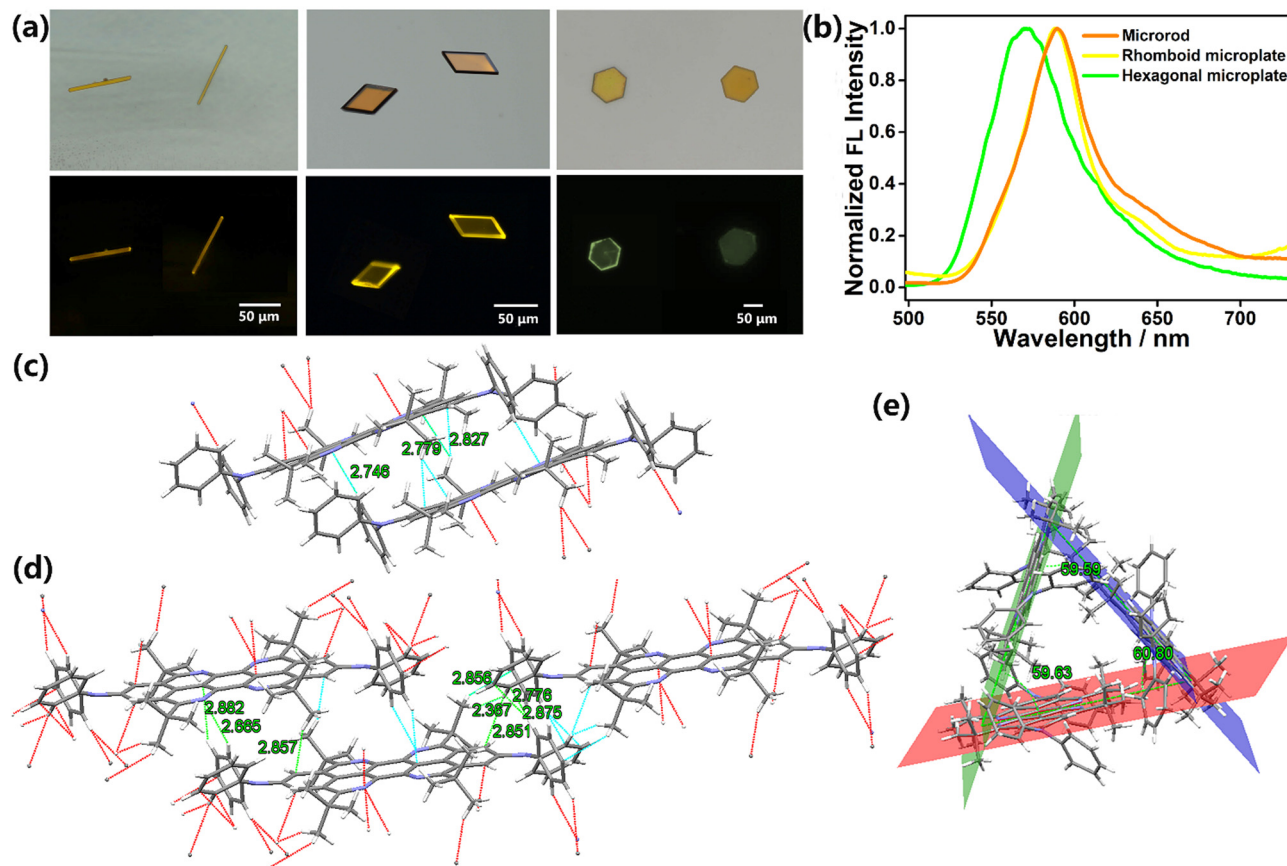
Fig. 2 (a) Bright–field optical (top) and fluorescence microscopy images (bottom), (b) normalized FL emission spectra of 1D microrods and 2D rhomboid and 2D hexagonal microplates. Molecular packing mode and multiple intermolecular interactions of (c) 1D microrods, (d) 2D rhomboid microplates as well as (e) 2D hexagonal microplates.

was therefore identified as a result of photo-induced electron transfer from the electron-rich peripheral DPA units (*i.e.*, the HOMO) to the electron-deficient TAPP core (*i.e.*, the LUMO), which differed from the results of **c-TAPP-T** displaying highly delocalized frontier orbitals. In addition, both the calculated and experimental results verified a narrower band gap concurrent with the elevation of the HOMO level for **c-TAPP-DPA** as compared to **c-TAPP-T** (Fig. S3, Table S1, ESI†). These findings were in line with the fact that electron-donating substituents in principle can influence the HOMO to a greater extent than the LUMO.[46]

Geometrically well-defined single crystals of **c-TAPP-DPA**, such as 1D microrods, and 2D rhomboid and hexagonal microplates, could be cultivated by solvent diffusion method at different liquid–liquid interfaces (Fig. 2a). For instance, the selection of methanol/dichloromethane and methanol/tetrahydrofuran led to microrods and rhomboid microplates, respectively. They both belonged to the triclinic $P\bar{1}$ space group (Table S2 and S3, ESI†). A closer inspection of their packing modes revealed that the microrods and rhomboids possessed a similar lamellar stacking manner yet showed differences in their layer-to-layer spacing, unit cell components and intermolecular interactions. In the two kinds of crystals, the aromatic cores aligned in parallel and far away from each other (9.920 Å, 9.943 Å in Fig. S4a and b, ESI†). The layer-to-layer spacing for

microrods and rhomboids was estimated to be 4.814 and 4.935 Å, respectively. Remarkably, as shown in Fig. S4c (ESI†) and Fig. 2c, the unit cell of microrods contained one molecule with multiple intermolecular interactions, such as C–H (DPA)···N (2.746 Å) and C–H (*t*-Bu)···C (peropyrene ring) (2.779 Å, 2.827 Å) were the main driving force of the microrods. In contrast, as for rhomboid microplates, each unit cell involved two molecules with more intense intermolecular interactions, including C–H (DPA)···N (2.665 Å) and C–H (*t*-Bu)···C (peropyrene ring) (2.857 Å), C–H (DPA)···C (peropyrene ring) (2.882 Å), C–H (DPA)···C (peropyrene ring) (2.851 Å), C–H (DPA)···C–H (*t*-Bu) (2.367 Å), C (DPA)···C–H (*t*-Bu) (2.856 Å) and C–H (DPA)···C (DPA) (2.776 Å, 2.875 Å) (Fig. 2d and Fig. S4d, ESI†).

On the other hand, hexagonal microplates were prepared from methanol and tetrahydrofuran, and the amount of methanol was less than that of preparing rhomboid microplates (details in the ESI†). Single crystal X-ray diffraction analyses verified that these hexagonal microplates adopted a completely different space group and molecular stacking style. In detail, the microplates belonged to the monoclinic *Cc* space group with three molecules crystalized into an equilateral triangle packing pattern, driven by the multiple intermolecular interactions (C–H (DPA)···C–H (*t*-Bu) (2.197–2.377 Å), C–H (DPA)···C (*t*-Bu) (2.704 Å, 2.857 Å), C–H (*t*-Bu)···C (peropyrene ring)

6140 | *J. Mater. Chem. C*, 2023, **11**, 6138–6144

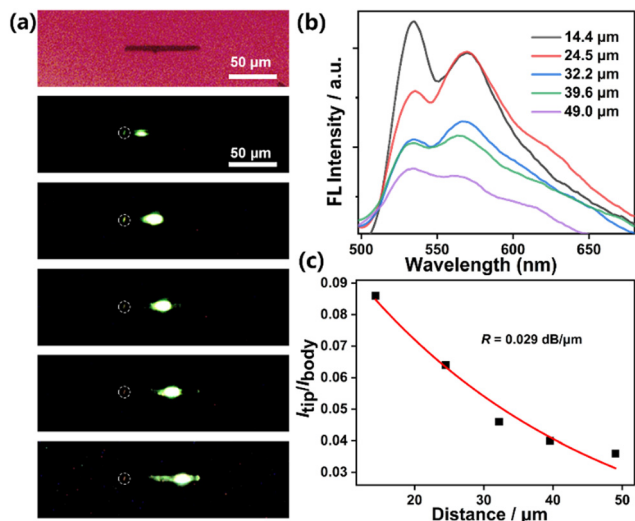This journal is © The Royal Society of Chemistry 2023

Fig. 3 (a) Bright-field and FL images obtained from a single **c-TAPP-DPA** 1D microrod by exciting the microrod at different positions. (b) Spatially resolved FL spectra from the tip of the microrod for different separation distances between the excitation spot and tip of the microrod shown in (a). (c) The intensity I_{tip}/I_{body} against the distance X corresponding to (a).

(2.781–2.899 Å), C–H (t-Bu)$\cdots$C–H (t-Bu) (2.324 Å)) (Table S4 and Fig. 2e and Fig. S5a and b, ESI†). The adjacent trimers arranged parallel to each other to form a 3D packing pattern under the intermolecular interactions of C–H (DPA)$\cdots$C (DPA) and C–H (t-Bu)$\cdots$C (peropyrene ring) (Fig. S5c and d, ESI†). Such a novel stacking mode endowed the hexagonal microplates with different FL properties compared to microrods and

rhomboids. As presented in Fig. 2b, the two layered crystals displayed yellow FL with an emission maximum at *ca.* 590 nm. In contrast, a hypsochromic shift of the emission band (20 nm) with brighter green FL (absolute quantum efficiency: 5.41%, Table S1, ESI†) was detected for hexagonal microplates. The excellent and differentiated emission behaviours of polymorphic **c-TAPP-DPA** crystals were in line with their single crystal structures. As illustrated in Fig. 2, the bulky DPA groups were twisted out of the tetraazaperopyrene plane. Moreover, these crystals have limited or even no π–π overlap areas between the neighbouring TAPP cores. The two factors inhibited intermolecular aggregation of **c-TAPP-T-DPA** perfectly, which was crucial for their efficient FL in the solid state. In particular, for the hexagonal microplates, the hypsochromic and brighter emission could be attributed to their equilateral triangle stacking mode, which reduces the overlap area between molecules as well as weakens the intermolecular interactions and dipole–dipole interaction. Simultaneously, the looser stacking of hexagonal crystals also endows them with a weaker ability to inhibit the vibration of diphenylamine substituents, making the FWHM of the FL spectrum for hexagonal microplates slightly broader than those of microrod and rhomboid microplates. Collectively, these findings highlighted the ability of **c-TAPP-DPA** to fabricate polymorphic microcrystals with geometry dependent FL properties, mostly derived from the well controls of multiple intermolecular interactions and twisting effect provided by the DPA substituents on a TAPP core.

To verify the versatility of these crystals as photonic materials, spatially resolved FL spectra of an individual microrod and
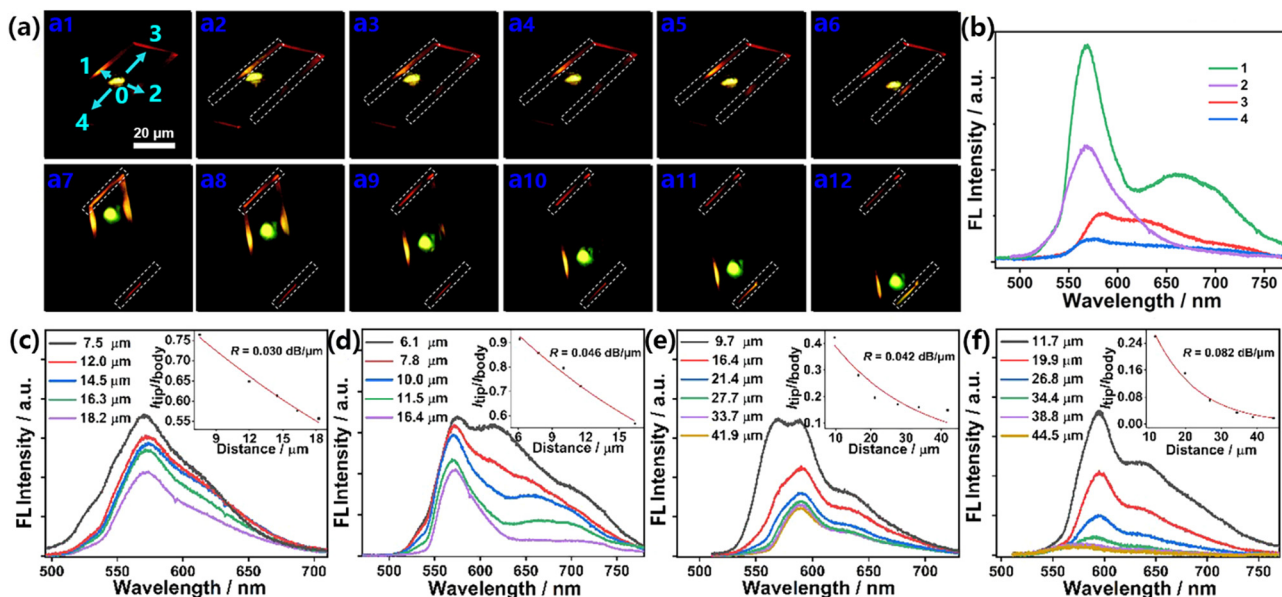

Fig. 4 (a) FL images obtained from a single 2D **c-TAPP-DPA** rhomboid microplate by exciting (a_1) the center, different positions in a2–a6) direction $\overrightarrow{01}$ and $\overrightarrow{02}$, (a7–a12) direction $\overrightarrow{03}$ and $\overrightarrow{04}$ with a UV laser (l = 375 nm). (b) The corresponding spatially resolved FL spectra of the excited spot and the four edges (marked with 1–4) of the microplate shown in (a_1). Spatially resolved FL spectra from the (c) edge 1, (d) edge 2, (e) edge 3, and (f) edge 4 of the **c-TAPP-DPA** rhomboid microplate for different separation distances between the excitation spot and the edge. The inset: Nonlinear fitting curve of optical waveguide loss. R: the optical loss coefficient.

This journal is © The Royal Society of Chemistry 2023

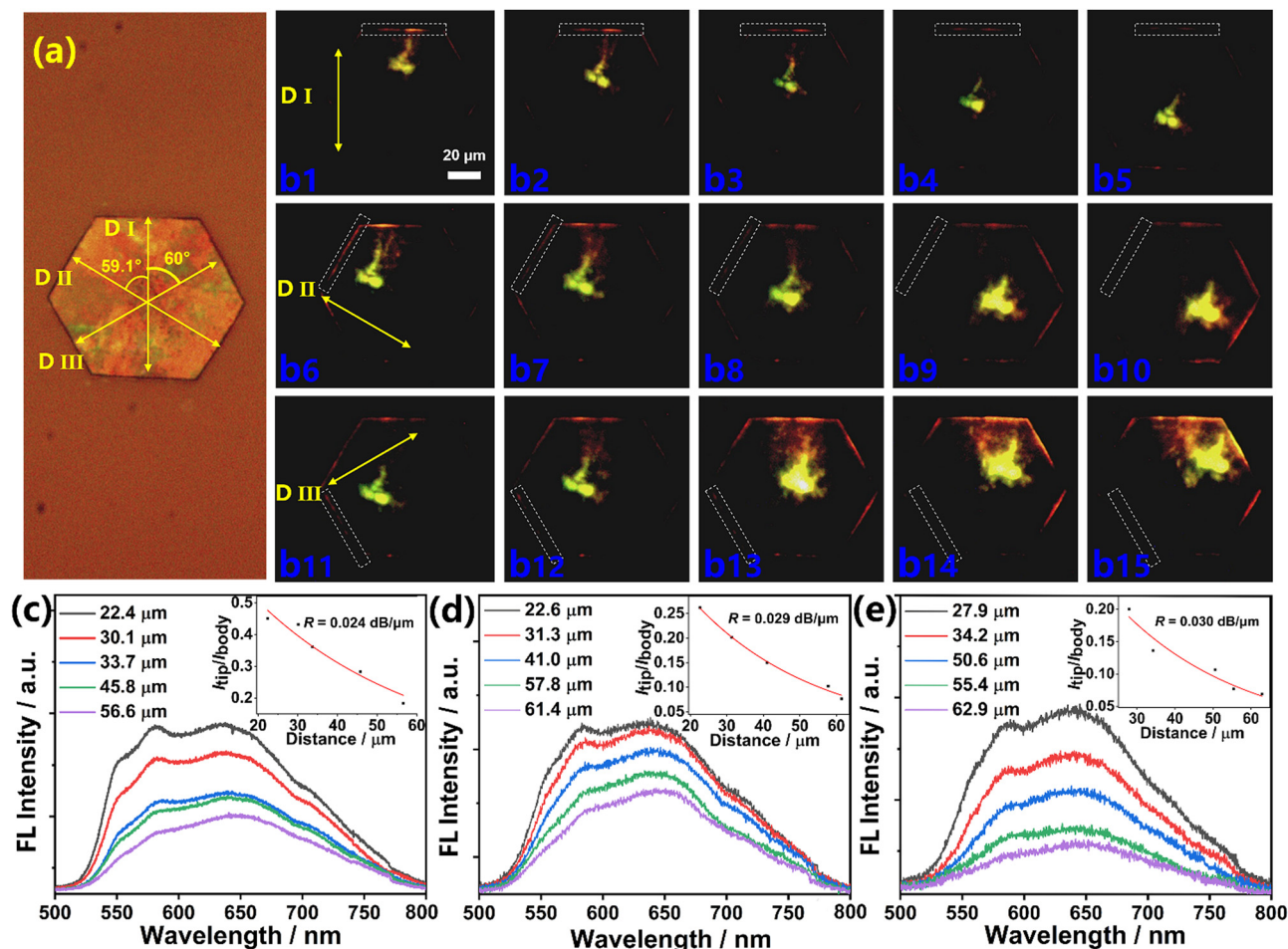*J. Mater. Chem. C*, 2023, **11**, 6138–6144 | **6141**

Fig. 5 (a) Bright-field images obtained from a single **c-TAPP-DPA** 2D hexagonal microplate. (b) Microarea FL images obtained by exciting an identical **c-TAPP-DPA** hexagonal microplate at different positions in direction I (b1–b5), direction II (b6–b10) and direction III (b11–b15). Spatially resolved FL spectra from the edge of the **c-TAPP-DPA** hexagonal microplate for different separation distances between the excitation spot and the edge in (c) direction I, (d) direction II and (e) direction III. The inset: Nonlinear fitting curve of optical waveguide loss. R: the optical loss coefficient.

microplate were recorded by locally exciting the crystal with a focused laser beam (λ = 375 nm). As for the microrods, when excited by focused laser at different positions, yellow emission was observed at the tip of the crystal (Fig. 3a). The FL spectra of the excitation site (body) and the tip site (tip) are shown in Fig. 3b. The intensity of output light decreased exponentially as a function of the propagation distance between the tip and the excitation point, signifying a characteristic feature of the 1D optical waveguide. Similar to many reported organic microcrystals, a relatively low optical loss coefficient (R) of 0.029 dB μm^{-1} was estimated according to the emission peaks located at 534 nm with the strongest intensity (Fig. 3c), indicating that FL energy can propagate efficiently along the axial direction of the microrods.

Interestingly, in the case of rhomboid microplates, the photons can propagate within the 2D plane featuring a less explored, asymmetric waveguide behavior. Typically, when the laser beam was focused at the center of the microplate with an edge length of about 20 μm × 48 μm, the FL microscopic images showed asymmetric FL in the four edges, *i.e.* the out-coupled beams of the two adjacent outcoupled edges

(1 and 3) were large and bright, while the opposite ones (2 and 4) were small and obscure (Fig. 4a1). The corresponding FL spectra of the four edges also quantitatively demonstrated that the propagation efficiencies of these microplates were highly sensitive to the propagation direction. That was, the emission intensities of edges 1 and 3 were about 1.5 times stronger than that of 2 and 4 (Fig. 4b and Fig. S6, ESI†). Interestingly, the FL spectra of different axial tips (1,2 and 3,4) also present distinct vibration peaks, which may be related to the slightly different arrangement of molecules within the micro-areas selected for testing. In each direction, the intensity of out-coupled light decreased exponentially as a function of propagation distance by changing the position of the excitation point. Accordingly, the loss coefficient R was determined to be 0.030 dB μm^{-1}, 0.046 dB μm^{-1}, 0.042 dB μm^{-1} and 0.082 dB μm^{-1} for the propagation path towards direction $\overrightarrow{01}$, $\overrightarrow{02}$, $\overrightarrow{03}$ and $\overrightarrow{04}$, respectively (Fig. 4a2–a12 and c–f). Smaller R values corresponding to the directions of $\overrightarrow{01}$ and $\overrightarrow{03}$ than those for the directions of $\overrightarrow{02}$ and $\overrightarrow{04}$ confirmed the 2D anisotropic transmission behavior in this rhomboid microcrystal. Very likely, this

6142 | *J. Mater. Chem. C*, 2023, **11**, 6138–6144

This journal is © The Royal Society of Chemistry 2023

asymmetric light propagation was due to the suitably aligned transition dipole of the oriented molecules with the incident light in the directions of $\overrightarrow{01}$ and $\overrightarrow{03}$, and *vice versa*. Such an anisotropic flow of photons occurring in the bright emissive microplate was appealing for the promising application of this kind of microcrystals in optical planar diodes.

Lastly, as for the hexagonal microplates, three-directional (D_I–D_{III}) 2D optical waveguide was determined. As shown in Fig. 5a and b1–b15, when the laser beam was focused on the hexagon (edge length of the crystal about 55 μm), photons propagated from center to the edges in three directions, and the out-coupled beams of the two opposite outcoupled edges in each direction showed slight difference, which may be related to the different output angles at two opposite edges.[38] Furthermore, in line with the hexagon shape, each propagation vector formed an angle of about 60° with the other two directions (Fig. 5a). The corresponding spatially resolved FL spectra in three directions were obtained by changing the input position on the microplate. In a similar way, $R_{I–III}$ representing the light dissipation during propagation along three directions were calculated as 0.024, 0.029 and 0.030 dB μm^{-1}, respectively (Fig. 5c–e). The approximately identical R values in different directions manifested an isotropic, multi-directional 2D waveguide performance, which implied a homogeneity of the crystal structure with well aligned molecules.

Conclusions

A new D–A type fluorophore consisting of a 5,6,12, 13-tetraazaperopyrene core and two DPA substituents at the 2,9-positions has been synthesized (**c-TAPP-DPA**). Flexibly twisted and electron rich DPA groups were essential to tune the intermolecular interactions and packing modes of **c-TAPP-DPA**. As a result, three kinds of microcrystals with different geometries (1D microrods, 2D rhomboid microplates and 2D hexagonal microplates) and FL properties (yellow *vs.* brighter green FL) were obtained. The polymorphism of the three microcrystals was found to be pertinent to different molecular interactions and arrangements of the molecules, and ultimately brought about geometry-dependent multi-dimensional/directional optical waveguide properties with low optical loss coefficient. In particular, the 2D rhomboid microplates displayed interesting asymmetric light propagation. Therefore, the polymorphic **c-TAPP-DPA** microcrystals have provided an excellent platform to study the relationship between molecular stacking patterns and solid-state optical and photonic properties. Furthermore, the ability to propagate light asymmetrically makes this kind of crystal a promising candidate for optically planar diodes and integrated photonic circuits.

Conflicts of interest

The authors declare no competing financial interest.

Acknowledgements

References

1 C. Zhang, Y. L. Yan, J. N. Yao and Y. S. Zhao, *Adv. Mater.*, 2013, **25**, 2854–2859.

2 W. Yao, Y. L. Yan, L. Xue, C. Zhang, G. P. Li, Q. D. Zheng, Y. S. Zhao, H. Jiang and J. N. Yao, *Angew. Chem., Int. Ed.*, 2013, **52**, 8713–8717.

3 Y. J. Li, Y. L. Yan, Y. S. Zhao and J. N. Yao, *Adv. Mater.*, 2016, **28**, 1319–1326.

4 C. Zhang, Y. L. Yan, Y. S. Zhao and J. N. Yao, *Acc. Chem. Res.*, 2014, **47**, 3448–3458.

5 H. Y. Liu, X. Q. Cao, Y. S. Wu, Q. Liao, A. J. Jiménez, F. Würthner and H. B. Fu, *Chem. Commun.*, 2014, **50**, 4620–4623.

6 L. Catalano, D. P. Karothu, S. Schramm, E. Ahmed, R. Rezgui, T. J. Barber, A. Famulari and P. Naumov, *Angew. Chem., Int. Ed.*, 2018, **57**, 17254–17258.

7 D. Tian and Y. L. Chen, *Adv. Opt. Mater.*, 2021, **9**, 2002264.

8 M. Luo, J. Zhao, Y. Y. Liu, L. Jiang, S. Wang and Z. G. Chi, *Adv. Opt. Mater.*, 2022, **10**, 2101227.

9 S. Q. Wu, B. Zhou and D. P. Yan, *Adv. Opt. Mater.*, 2021, **9**, 2001768.

10 X. M. Lu, X. D. Wang, Q. Liao and H. B. Fu, *J. Phys. Chem. C*, 2015, **119**, 22108–22113.

11 X. D. Wang, Q. Liao, X. M. Lu, H. Li, Z. Z. Xu and H. B. Fu, *Sci. Rep.*, 2014, **4**, 7011.

12 X. D. Wang, Q. Liao, Q. H. Kong, Y. Zhang, Z. Z. Xu, X. M. Lu and H. B. Fu, *Angew. Chem., Int. Ed.*, 2014, **53**, 5863–5867.

13 W. Zhang, J. N. Yao and Y. S. Zhao, *Acc. Chem. Res.*, 2016, **49**, 1691–1700.

14 X. D. Wang, Z. Z. Li, M. P. Zhuo, Y. S. Wu, S. Chen, J. N. Yao and H. B. Fu, *Adv. Funct. Mater.*, 2017, **27**, 1703470.

15 W. Zhang, Y. L. Yan, J. M. Gu, J. N. Yao and Y. S. Zhao, *Angew. Chem., Int. Ed.*, 2015, **54**, 7125–7129.

16 Y. G. Zhen, H. L. Dong, L. Jiang and W. P. Hu, *Chin. Chem. Lett.*, 2016, **27**, 1330–1338.

17 D. Liu, C. G. Li, S. J. Niu, Y. Li, M. X. Hu, Q. Y. Li, W. G. Zhu, X. T. Zhang, H. L. Dong and W. P. Hu, *J. Mater. Chem. C*, 2019, **7**, 5925–5930.

18 S. Z. Bisri, T. Takenobu, Y. Yomogida, H. Shimotani, T. Yamao, S. Hotta and Y. Iwasa, *Adv. Funct. Mater.*, 2009, **19**, 1728–1735.

19 J. Li, K. Zhou, J. Liu, Y. G. Zhen, L. Liu, J. D. Zhang, H. L. Dong, X. T. Zhang, L. Jiang and W. P. Hu, *J. Am. Chem. Soc.*, 2017, **139**, 17261–17264.

20 Y. S. Zhao, H. B. Fu, A. D. Peng, Y. Ma, D. B. Xiao and J. N. Yao, *Adv. Mater.*, 2008, **20**, 2859–2876.

21 Y. S. Zhao, H. B. Fu, F. Q. Hu, A. D. Peng, W. S. Yang and J. N. Yao, *Adv. Mater.*, 2008, **20**, 79–83.

22 M. W. Li, Y. Yuan and Y. L. Chen, *Chin. J. Chem.*, 2021, **39**, 3101–3115.

23 W. Yuan, X. K. Ren, M. W. Li, H. S. Guo, Y. Han, M. J. Wu, Q. Wang, M. M. Li and Y. Chen, *Angew. Chem., Int. Ed.*, 2018, **57**, 6161–6165.

24 C. Wang and Z. Li, *Mater. Chem. Front.*, 2017, **1**, 2174–2194.

25 S. Q. Ma, Y. J. Liu, J. B. Zhang, B. Xu and W. J. Tian, *J. Phys. Chem. Lett.*, 2020, **11**, 10504–10510.

26 C. Zhang, Y. L. Yan, Y. Y. Jing, Q. Shi, Y. S. Zhao and J. N. Yao, *Adv. Mater.*, 2012, **24**, 1703–1708.

27 W. Yao and Y. S. Zhao, *Nanoscale*, 2014, **6**, 3467–3473.

28 Q. Li, Y. Jia, L. R. Dai, Y. Yang and J. B. Li, *ACS Nano*, 2015, **9**, 2689–2695.

29 K. Wang, H. Y. Zhang, S. Y. Chen, G. C. Yang, J. B. Zhang, W. J. Tian, Z. M. Su and Y. Wang, *Adv. Mater.*, 2014, **26**, 6168–6173.

30 Y. Yu, Y. C. Tao, S. N. Zou, Z. Z. Li, C. C. Yan, M. P. Zhuo, X. D. Wang and L. S. Liao, *Sci. China: Chem.*, 2020, **63**, 1477–1482.

31 Z. Z. Xu, Z. W. Zhang, X. Jin, Q. Liao and H. B. Fu, *Chem. – Asian J.*, 2017, **12**, 2985–2990.

32 H. Zhang, D. Jin, D. Q. Lin, L. Huang, J. Wang, S. S. Wang and L. H. Xie, *Chin. J. Chem.*, 2022, **40**, 832–837.

33 X. Ye, Y. Liu, Q. Guo, Q. X. Han, C. Ge, S. Y. Cui, L. L. Zhang and X. T. Tao, *Nat. Commun.*, 2019, **10**, 761.

34 X. D. Zhang, J. Y. Gong, W. Tao, X. J. Jiang, C. Chen and P. F. Wei, *ACS Mater. Lett.*, 2022, **4**, 1468–1474.

35 J. Wang, S. P. Xu, A. S. Li, L. Chen, W. Q. Xu and H. Y. Zhang, *Mater. Chem. Front.*, 2021, **5**, 1477–1485.

36 L. P. Heng, X. Y. Wang, D. L. Tian, J. Zhai, B. Z. Tang and L. Jiang, *Adv. Mater.*, 2010, **22**, 4716–4720.

37 Z. Q. Li, D. X. Ma, F. F. Xu, T. X. Dan, Z. L. Gong, J. Y. Shao, Y. S. Zhao, J. N. Yao and Y. W. Zhong, *Angew. Chem., Int. Ed.*, 2022, **61**, e202205033.

38 Y. Liu, H. P. Hu, L. Xu, B. Qiu, J. Liang, F. Ding, K. Wang, M. M. Chu, W. Zhang, M. Ma, B. Chen, X. Z. Yang and Y. S. Zhao, *Angew. Chem., Int. Ed.*, 2020, **59**, 4456–4463.

39 Q. Li, W. Jin, M. M. Chu, W. Zhang, J. M. Gu, B. Shahid, A. B. Chen, Y. F. Yu, S. L. Qiao and Y. S. Zhao, *Nanoscale*, 2018, **10**, 4680–4685.

40 M. P. Zhuo, Y. C. Tao, X. D. Wang, Y. C. Wu, S. Chen, L. S. Liao and L. Jiang, *Angew. Chem., Int. Ed.*, 2018, **57**, 11300–11304.

41 J. Wang, S. T. Zhang, S. P. Xu, A. S. Li, B. Li, L. Ye, Y. J. Geng, Y. Tian and W. Q. Xu, *Adv. Opt. Mater.*, 2020, **8**, 1901280.

42 M. Q. Dai, B. Zhou, X. Y. Fang and D. P. Yan, *ACS Appl. Mater. Interfaces*, 2022, **14**, 40223–40231.

43 N. Chandrasekhar and R. Chandrasekar, *Angew. Chem., Int. Ed.*, 2012, **51**, 3556–3561.

44 H. W. Luo, S. J. Chen, Z. T. Liu, C. Zhang, Z. X. Cai, X. Chen, G. X. Zhang, Y. S. Zhao, S. Decurtins, S. X. Liu and D. Q. Zhang, *Adv. Funct. Mater.*, 2014, **24**, 4250–4258.

45 W. Yuan, J. J. Cheng, X. P. Li, M. J. Wu, Y. Han, C. M. Yan, G. Zou, K. Mullen and Y. L. Chen, *Angew. Chem., Int. Ed.*, 2020, **59**, 9940–9945.

46 S. Geib, S. C. Martens, M. Marken, A. Rybina, H. Wadepohl and L. H. Gade, *Chem. – Eur. J.*, 2013, **19**, 13811–13822.

6144 | *J. Mater. Chem. C*, 2023, **11**, 6138–6144

This journal is © The Royal Society of Chemistry 2023